LA-13683-MS

Regenerative Fuel Cell Engineering – FY99

Los Alamos
NATIONAL LABORATORY

Los Alamos National Laboratory is operated by the University of California for the United States Department of Energy under contract W-7405-ENG-36.

This work was supported by the US Department of Energy, Office of Energy Efficiency and Renewable Energy, Office of Power Technologies, Hydrogen Programs.

An Affirmative Action/Equal Opportunity Employer

LA-13683-MS

Issued: January 2000

Regenerative Fuel Cell Engineering – FY99

Michael A. Inbody
Rodney L. Borup
James C. Hedstrom
Jose Tafoya
Byron Morton
*Lois Zook**
*Nicholas E. Vanderborgh***

**Delta State University, Box 3225, 180D Walters, 1008 College St., Cleveland, MS 38733*
***Blue Star Industries Corp., 12600 West Colfax Ave., Suite C-501, Lakewood, CO 80215*

Los Alamos
NATIONAL LABORATORY
Los Alamos, New Mexico 87545

Contents

List of Figures

List of Tables

Regenerative Fuel Cell Engineering – FY99

Michael A. Inbody, Rodney L. Borup, James C. Hedstrom, José Tafoya,
Byron Morton, Lois Zook, and Nicholas E. Vanderborgh

1.0 Abstract

We report the work conducted by the ESA-EPE Fuel Cell Engineering Team at Los Alamos National Laboratory during FY99 on regenerative fuel cell system engineering. The work was focused on the evaluation of regenerative fuel cell system components obtained through the RAFCO program. These components included a 5 kW PEM electrolyzer, a two-cell regenerative fuel cell stack, and samples of the electrolyzer membrane, anode, and cathode. The samples of the electrolyzer membrane, anode, and cathode were analyzed to determine their structure and operating characteristics. Tests were conducted on the two-cell regenerative fuel cell stack to characterize its operation as an electrolyzer and as a fuel cell. The 5 kW PEM electrolyzer was tested in the Regenerative Fuel Cell System Test Facility. These tests served to characterize the operation of the electrolyzer and, also, to verify the operation of the newly completed test facility. Future directions for this work in regenerative fuel cell systems are discussed.

2.0 Introduction

We report the work conducted by the ESA-EPE Fuel Cell Engineering Team at Los Alamos National Laboratory during FY99 on regenerative fuel cell system engineering. This work included development of a Regenerative Fuel Cell Test Facility and evaluation of an electrolyzer and a regenerative fuel cell obtained from Vladimir Fateev of the RRC Kurchatov Institute in Moscow.

The motivation for this work in regenerative fuel cell system engineering is the development of a mechanism for energy storage and retrieval for alternative energy systems. This energy storage and retrieval is a critical element of developing alternative energy technologies such as wind and solar. Photovoltaic and wind sources are now being quickly commercialized globally. These discrete sources are inherently transient and require integrated energy storage. Usually chemical batteries are utilized for this purpose. Batteries turn out almost always to be the component which limits system effectiveness. Improved energy storage devices are critical components. The design criteria for these are 1) consumer products fabricated with no toxic or dangerous agents; 2) high reliability; 3) long lifetime, preferably as long as the lifetime of the energy generating component (30 years for PV arrays); 4) minimal maintenance; 5) acceptable cost; and 6) high efficiency. The most common energy storage component today, lead acid batteries, meet only the last criterion.

Regenerative fuel cells (RFC) are not a new idea, but a good one. The concept is to operate a fuel cell both in the forward mode (electricity production from stored reactants) and the

reverse mode (reactant production from excess electricity). In some ways an RFC is identical to a secondary battery. However there are important differences. As with all fuel cell systems, the energy and power parameters are separated. The quantity of energy stored is a function of the reactant storage volume. Reactant storage volume is inexpensive contrasted to battery energy storage. An RFC system is inherently modular and one system can be configured to achieve many different design goals. Therefore it is no surprise that RFC systems have had considerable research and development during the last 20 years.

Hydrogen-oxygen systems remain attractive because of the non-toxic nature of the reactants. Engineering toxins such as bromine, chlorine, lead, cadmium, etc. into a long-lived consumer product raises many costly concerns. However hydrogen-oxygen systems today demonstrate disappointing efficiency. This remains an important research topic, with great progress in achieving viable systems. Fuel cell engineering has resulted in far improved performance during the last decade. Opportunities for improving electrolyzer voltage performance remain. Useful 3-dimensional models exist for these devices. With appropriate measurements compared to predictions from these models, there is high probability that the cause for efficiency loss will be understood. And then, with that understanding, engineering solutions hopefully will be apparent. Even so, today's hardware meeting the above design criteria is useful. Inefficiency in both the fuel cell mode and the electrolysis mode results in heat, which can be used for hot water heating and for space heating/cooling. A well-designed building system that is integrated into modern buildings can utilize large fractions of the "waste" heat.

During FY98, work at Los Alamos National Laboratory led the fuel cell engineering community by building new diagnostic tools for PEM electrolyzers. Previously, with DOE support beginning in 1978, LANL had developed unique designs for PEM fuel cell stack test hardware, supplemented by computer control systems and advanced performance models. This hardware is in daily use at major US corporations such as General Motors and DuPont Chemical. Based on that experience base, we crafted concepts for a new Regenerative Fuel Cell Test Facility that permits testing at a variety of currents, pressures, and temperatures and permits experimental simulation of a variety of reactant storage options. The development and fabrication of this facility was completed this year. Simultaneously Sandia National Laboratory worked to acquire regenerative fuel cell system components from a Russian company, the RRC Kurchatov Institute, under the auspices of the RAFCO program. These components included a 5 kW PEM electrolyzer, a two-cell regenerative fuel cell stack, and samples of the electrolyzer membrane, anode, and cathode. Scientists in the former Soviet Union have developed a range of new fuel cell technology. Part of this is a new, improved polymer that provides improved performance. This unit is configured with that material. The Russian scientists also developed new electrodes. Unlike US designs, these are made using stable graphite supports. Such a design would have a far lower cost and would be expected to show different operating dynamics.

The work completed this year is described below. An analysis of the samples of the Russian PEM electrolyzer components is described first. Next, we report a series of experiments conducted on the two-cell regenerative fuel cell stack. We describe the Regenerative Fuel Cell System Test Facility next. Then, we report the testing of the 5 kW PEM electrolyzer using the RFC System Test Facility. We conclude with planned future work.

3.0 Analysis of Russian PEM Electrolyzer Components

3.1 Introduction

Component parts for a proton exchange membrane water electrolyzer were obtained via the RAFCO program from Vladimir N. Fateev at RRC Kurchatov Institute Hepti. Two electrodes were shipped, a cathode coated with Pt catalyst, carbon, and ion exchange membrane material, and an anode consisting of Ir catalyst and membrane material. The support metal for both electrodes was porous Ti coated with a proprietary anti-corrosion layer. A Nafion type Russian membrane material MF-4SK was also shipped and tested.

A variety of tests were undertaken to evaluate the Russian electrolyzer components. The physical properties of the Russian membrane MF-4SK, such as polymer density, ion exchange capacity, and the mass transport rate of a redox probe through the polymer, were tested. These physical properties were compared to those of commercial Nafion 117 obtained from Aldrich Chemical Company. Both electrodes and the membrane material were visually inspected using a Nikon optical microscope. The anode, cathode, and membrane material were then sandwiched into an ElectroCell AB Micro Flow Cell and electrolysis experiments were performed on the system.

3.2 Physical Properties of the Russian Membrane versus Nafion 117

The dry density, the equivalent weight, and the mass transport properties of the Russian MF-4SK membrane and the Nafion 117 membrane were measured and compared. Dry density of the membrane was calculated from measured volumes and weights of membrane pieces. The ion exchange capacity as measured by the equivalent weight was determined by titration. The equivalent weight of the polymer is defined as the grams of polymer per mole of sulfonic acid groups available for ion exchange. The mass transport rate of a redox probe, hydroquinone, was measured using cyclic voltammetry. The average and standard deviation obtained from the measurements on three samples each of the Russian and Nafion membrane are presented in Table 3-1.

Table 3-1. Summary and Comparison of the Physical Property Measurements of the Russian Membrane MF-4SK and Nafion 117

Property	Russian Membrane MF-4SK	Nafion 117*
Dry Density	1.91 ± 0.08 g/cm3	2.06 ± 0.09 g/cm3
Average Equivalent Weight	1250 ± 40 g/mol	1220 ± 70 g/mol
Average Effective Flux	1.98 ± 0.14 × 10-3 mol/s	1.91 ± 0.25 × 10-3 mol/s

*Samples of Nafion 117 obtained from Aldrich Chemical Company.

The dry density, the ion exchange capacity, and the transport of the redox species, hydroquinone, of the Russian MF-4SK membrane and the Nafion 117 samples were determined to be equivalent to one another, within the margin of error for the measurement techniques.

3.3 Optical Microscopy

Samples of the anode, cathode, Russian membrane, and Nafion 117 were each cast in epoxy resin and examined using a Nikon optical microscope. The Russian membrane MF-4SK was observed under the Nikon optical microscope to determine whether the membrane was a solid film or if it was made by pressing a series of thinner laminate films. The polymer film looked to be a single solid film, rather than several thin layers of laminate, as shown in Figure 3-1. The film thickness was measured to be approximately 10 mil.

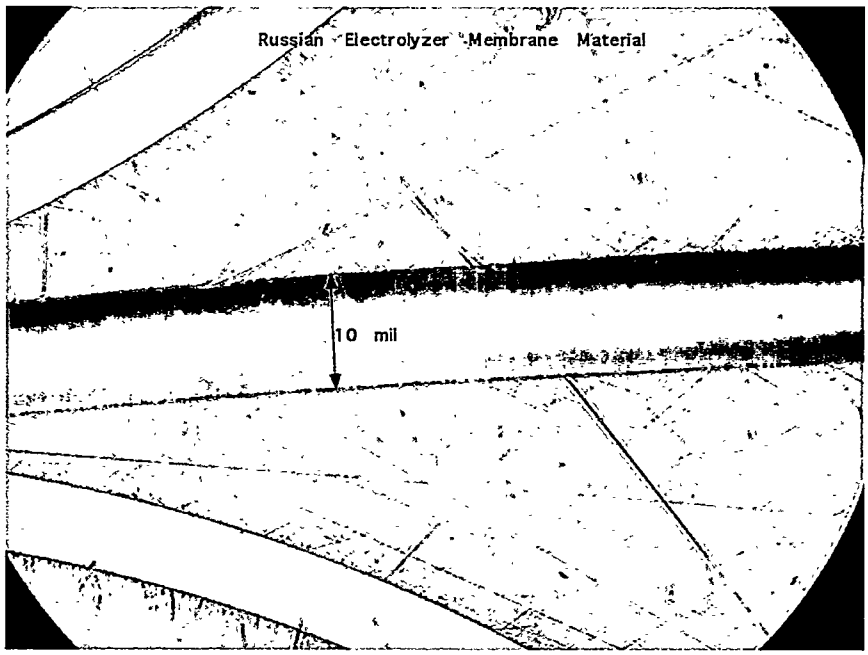

Figure 3-1. Russian electrolyzer membrane under Nikon optical microscope.

The anode and cathode also were examined under the optical microscope. Figure 3-2 shows the electrolyzer anode at 50X magnification. The porous nature of the Ti support is clearly visible. The entire anode thickness is approximately 50 mil, with the catalyst layer thickness being less than 1 mil. Figure 3-3 shows the cathode at 50X magnification. The dimensions are similar to those of the anode.

3.4 Micro Flow Cell Measurements

Electrolysis experiments were performed using the Russian electrolyzer components in an ElectroChem AB Flow Cell. Pieces of the Russian-supplied anode, cathode, and membrane were cut to fit the dimensions of the cell. The membrane material was sandwiched between the anode and the cathode, with the catalyzed sides of the electrodes in contact with the membrane. Silicon gasketing was used to mask off all but 10 cm^2 of the electrode area for both the cathode and anode, and was used to seal the cell. Water was supplied to the anode inlet with an HPLC pump with the anode and cathode exhaust vented separately. A potential was applied to the cell using a potentiostat with a current booster.

Optimal operating conditions were determined during initial experiments. Electrolyzer performance was not affected by variations in the water flow rate between 1 ml/min and 10 ml/min. A 5 ml/min water flow rate was maintained for all the subsequent experiments. Polarization curves were obtained using a cyclic voltammogram at a scan rate of 5 mV/s from 0 to 2.4 V. Polarization curves were repeated over several days with no degradation in performance over the time period of the tests. Polarization curves were measured at 20 °C, 40 °C, and 70 °C to investigate the effects of temperature on electrolysis performance. To maintain the temperature of the cell, water was preheated before entering the pump and the micro flow cell was placed in the column oven compartment of a GC. All the tests were conducted at ambient pressure (in Los Alamos, ~11.3 psia).

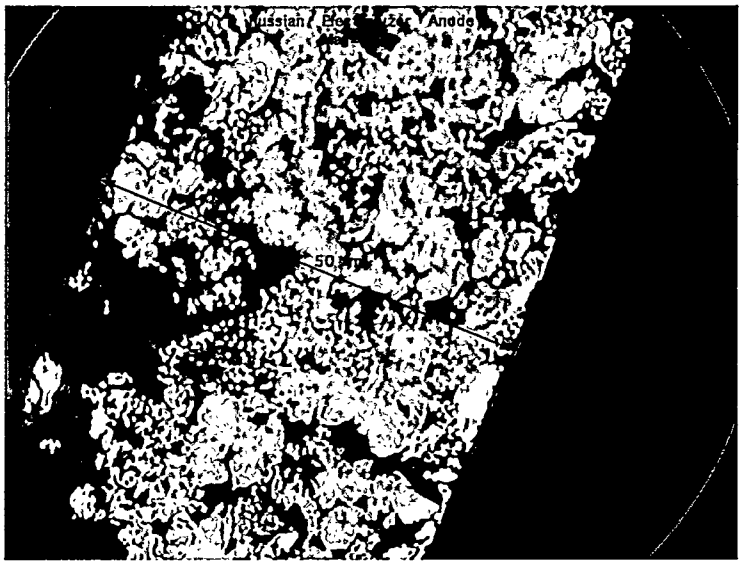

Figure 3-2. Russian electrolyzer anode at 50X magnification on Nikon microscope.

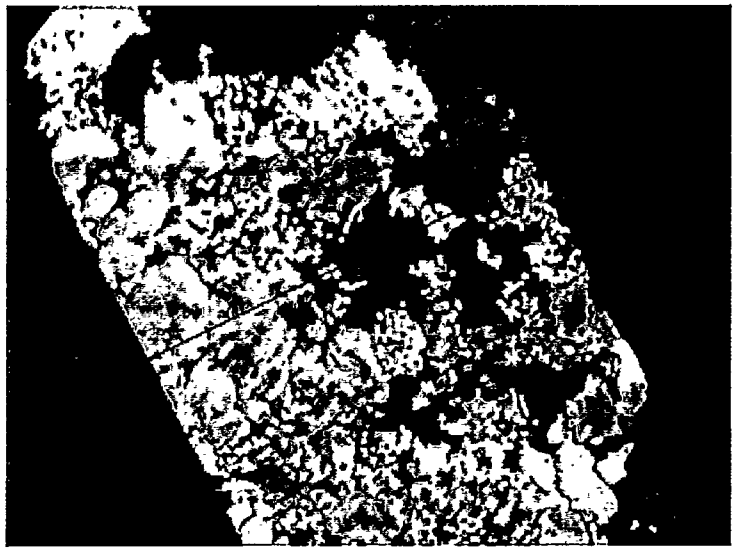

Figure 3-3. Russian electrolyzer cathode at 50X magnification on Nikon microscope.

Figure 3-4 shows the polarization curve, voltage vs. current density, obtained with the system operated at ambient conditions with a water flow rate of 5 ml/min. Over the potential range of 1.4–2.8V, the maximum current density was ~0.37 amps/cm^2. This number is in good agreement with the maximum current density reported by the Russians for their full-scale PEM electrolyzer, which was 0.4 amps/cm^2. In this case, we achieved close to the reported number at room temperature.

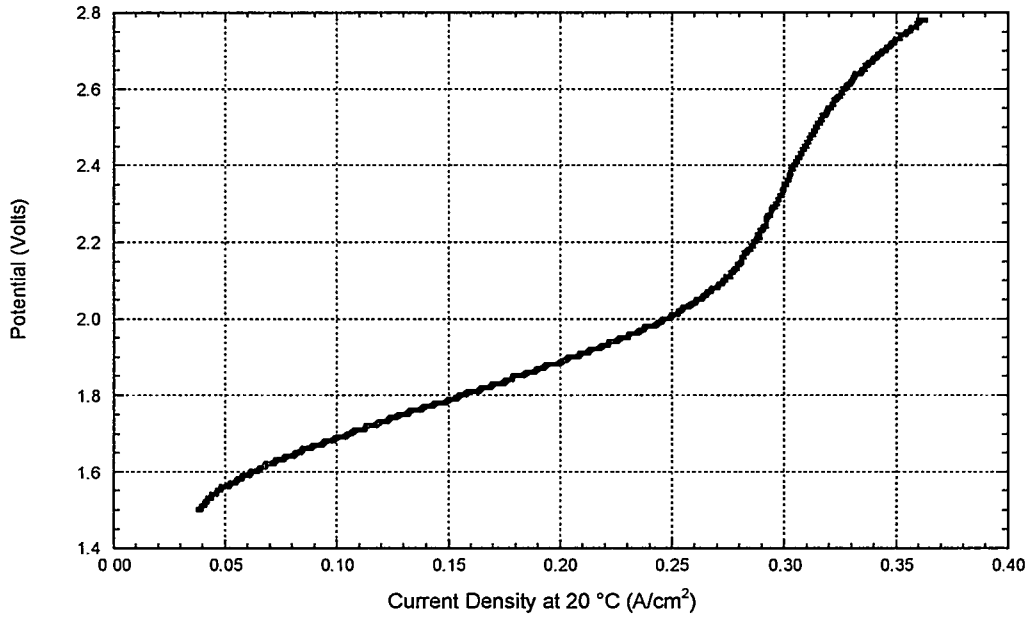

Figure 3-4. Water electrolysis polarization curve for micro flow cell with Russian components at ambient temperature and pressure.

Figure 3-5 shows the polarization curves for the electrolyzer components in the micro flow cell at 20 °C, 40 °C, and 70 °C. At voltages below ~2.0 V, the electrolysis cell performs about the same for each temperature. At the higher applied voltages, such as 2.8 volts, the current response at 20 °C was 3.63 A, at 40 °C the response was 4.13 A, and at 70 °C the response was 5.00 A.

The initial temperature increase from 20 °C to 40 °C enhanced performance approximately 15% over that of the ambient cell. The 50 °C temperature increase from 20 to 70 °C enhanced performance approximately 35% over that of the ambient cell. A linear regression of the temperature versus current data results in a line with a slope of 0.0275, an intercept of 3.06. The data set is limited, but over this temperature range, there appears to be a linear relationship between the current response and the operating temperature at the given potential. The current at 2.8 volts increased 0.275 amps for every 10 °C increase in operating temperature.

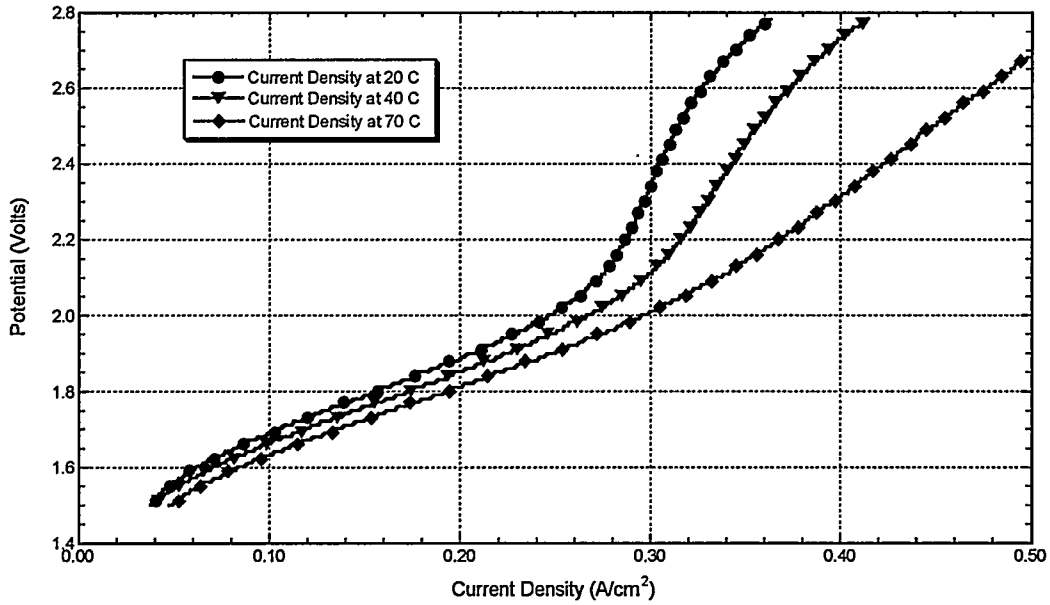

Figure 3-5. Temperature effects on the water electrolysis of the Russian electrolyzer components.

3.5 Summary

The Russian MF-4SK membrane material was found to have the same density, ion exchange capacity, and mass transport characteristics as Nafion 117 commercially available from Aldrich. The only difference found between the two materials tested was polymer film thickness, with the Russian polymer being 10 mil thick and the Nafion 117 being 7 mil thick. Under the optical microscope they appeared to be made by a similar process that results in a single thick film rather than a composite of thinner laminates.

The anode and cathode catalysts were made of very thin layers (< 1 mil) of metals attached to a 50 mil Ti support. The Ti layer was shown to be porous under the optical microscope, which would allow for the facile transport of water and gasses to and from the catalyst layers. The catalyst layers were somewhat intercalated into the porous Ti support. This intercalation is not readily visible in the micrographs in Figures 3-2 and 3-3, but on the larger TV screen monitor catalyst material could be seen both at the surface as well as along some of the interior Ti structures.

Electrolysis experiments on the component materials showed that the cell was capable of achieving a current density of approximately 0.4 amps/cm^2. This current density was achieved at ambient conditions in a non-optimized cell design, so this number is probably a conservative estimate of the capabilities of the system. A 5–10% increase in cell performance was observed for each 10 degree increment of cell operating temperature. The electrodes and the membrane material were in physical contact with one another, but no effort was made to improve the contact area between the catalyst layers and the polymer, so improvements could be made.

4.0 Regenerative Fuel Cell Stack

4.1 Introduction

The regenerative fuel cell is a small 25 cm^2 active area, 2-cell stack that can operate in electrolytic or fuel cell mode. The reversible fuel cell module consists of a Pt-Ir anode catalyst (2 mg/cm^2) supported by a platinized porous Ti current collector. Hydrophobic Pt on carbon (0.5 mg/cm^2) is used as a cathode catalyst. The cathode current collector is hydrophobic carbon cloth. The Russian-made membrane MF-4SK with a thickness of 145 microns is used as the electrolyte.

The two modes of operation of the regenerative fuel cell are shown in Figure 4-1. The fuel cell mode is shown at the left of Figure 4-1 with hydrogen oxidation occurring on the anode side, protons migrating across the membrane and reacting with reduced oxygen at the cathode. The electrolytic mode of operation is shown at the right of Figure 4-1. The oxidation of oxygen (from water) occurs on the anode side with protons migrating across the membrane, where the protons are reduced to form hydrogen.

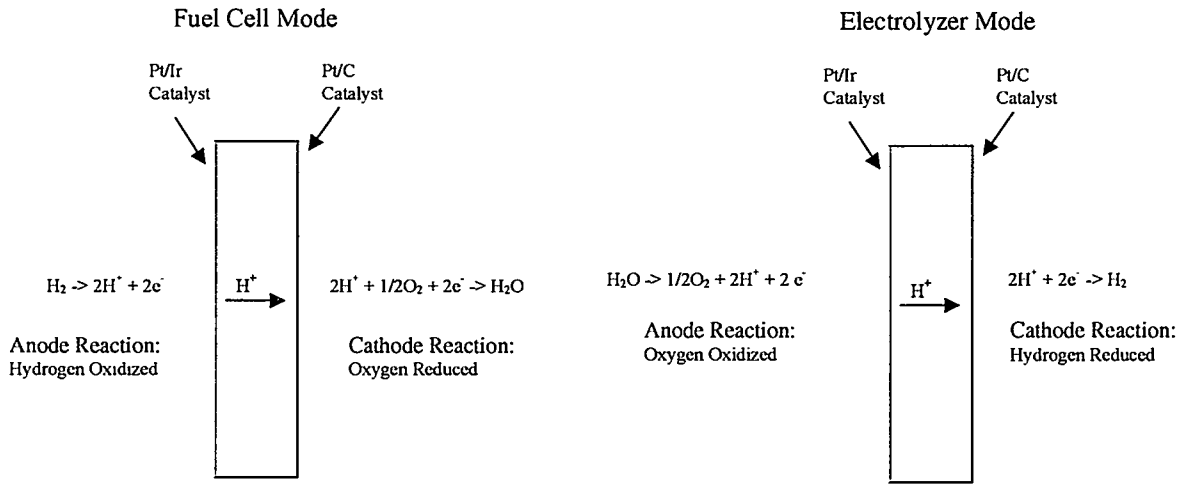

Figure 4-1. Schematic of the regenerative fuel cell operation.

Figure 4-2 shows the regenerative fuel cell stack. Three types of measurements were made on the 2-cell regenerative fuel cell stack: hydrogen adsorption/desorption, electrolysis polarization and fuel cell measurements. The separate measurements are described in detail below.

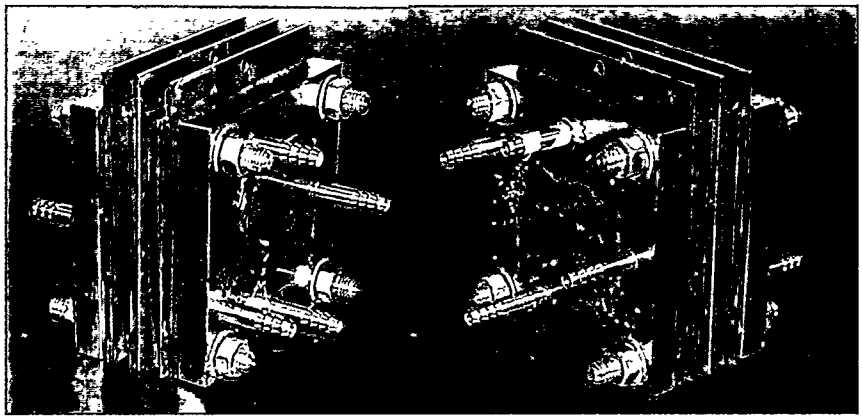

Figure 4-2. Two views of the 2-cell regenerative fuel cell stack. The picture on the left shows the hydrogen inlet and outlet ports. The picture on the right shows the oxygen inlet and outlet ports.

4.2 Hydrogen Adsorption/Desorption

The active surface area of the catalyst was measured by evaluating the hydrogen adsorption/desorption. For these measurements, the fuel cell cathode was exposed to nitrogen, while hydrogen was used on the anode side. The cathode was made the working electrode and the anode was used as both the reference and counter electrode. Hydrogen adsorption charge was obtained by integrating the current from the potential at which hydrogen desorption commences to about 0.4 V_{RHE} where only the double layer charge is present. The double layer capacitance was subtracted from the hydrogen adsorption curve by subtracting the double layer current that was observed for each individual voltammogram. After measurements were taken, the gases and electrodes were reversed to measure the surface area of the other side of the MEA. Polarization effects at the counter electrode were neglected since the hydrogen oxidation reaction at the fuel cell anode is nearly reversible. The electrochemical measurements were made using a Pine AFCBP1 Bi-Potentiostat interfaced with a computer for data acquisition. Sweep rates of 20 mV/sec and 50 mV/sec were used to acquire the voltammograms.

The cyclic voltammogram for the anode catalyst of cell 1 of the two-cell stack is shown in Figure 4-3. The voltammogram is typical for that of a platinum catalyst supported on an MEA for a fuel cell.[1] Hydrogen adsorption occurs on the negative sweep starting at about 0.35 V and continues until the catalyst surface is saturated with hydrogen, at which point H_2 evolution starts to occur (at potentials < 0.05 V). On the reverse positive sweep, hydrogen desorption occurs from the catalytic surface from about 0.1 V to 0.4 V. The region from 0.4 to 0.5 V is termed the "double layer region" because only capacitive charging is present. To measure the catalyst surface area, the double layer capacitance is subtracted, the hydrogen desorption is integrated, and the catalyst surface area is calculated. The catalyst surface area measured by this method for Figure 4-3 is 176 cm^2. Since the feed gas on the anode side of the MEA is nitrogen, the hydrogen adsorption that occurs is from protons produced on the other side of the MEA diffusing through the membrane. Thus, only the electrochemically active platinum available for the fuel cell reaction is measured.

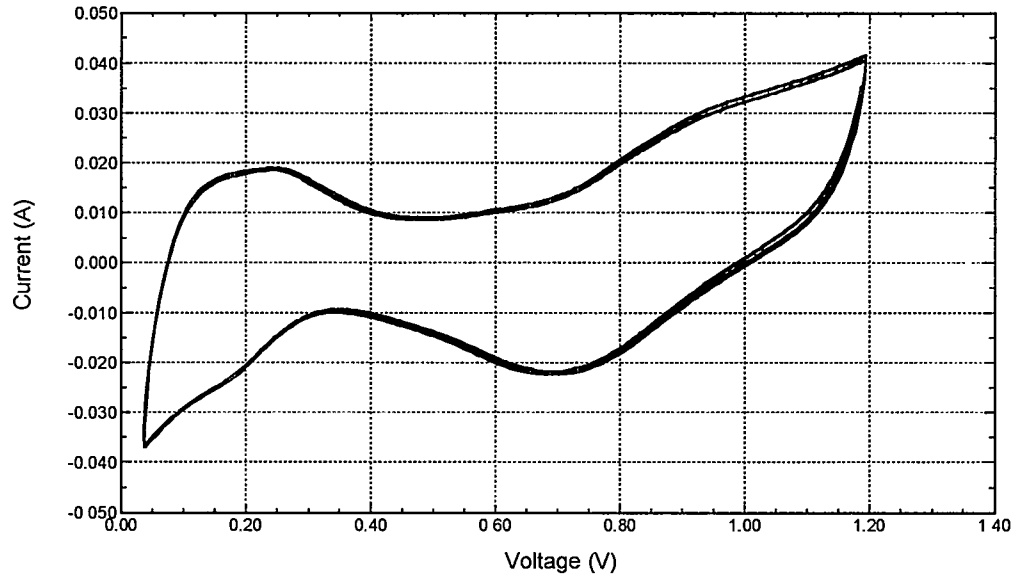

Figure 4-3. Hydrogen adsorption/desorption voltammogram for the anode catalyst of cell 1.

Figure 4-4 shows the voltammogram for the anode of cell 2. The voltammogram is similar in shape, with a higher surface area of 304 cm^2. Figures 4-5 and 4-6 show the hydrogen adsorption/desorption voltammograms for the cathodes of cells 1 and 2 respectively. Note that the shape of the adsorption/desorption is much less pronounced compared with the capacitance; thus the surface area is much lower at 4.5 and 11.1 cm^2. The active platinum surface area measured was low for the reported amount of Pt on the MEA. The surface areas for the four electrodes are summarized in Table 4-1.

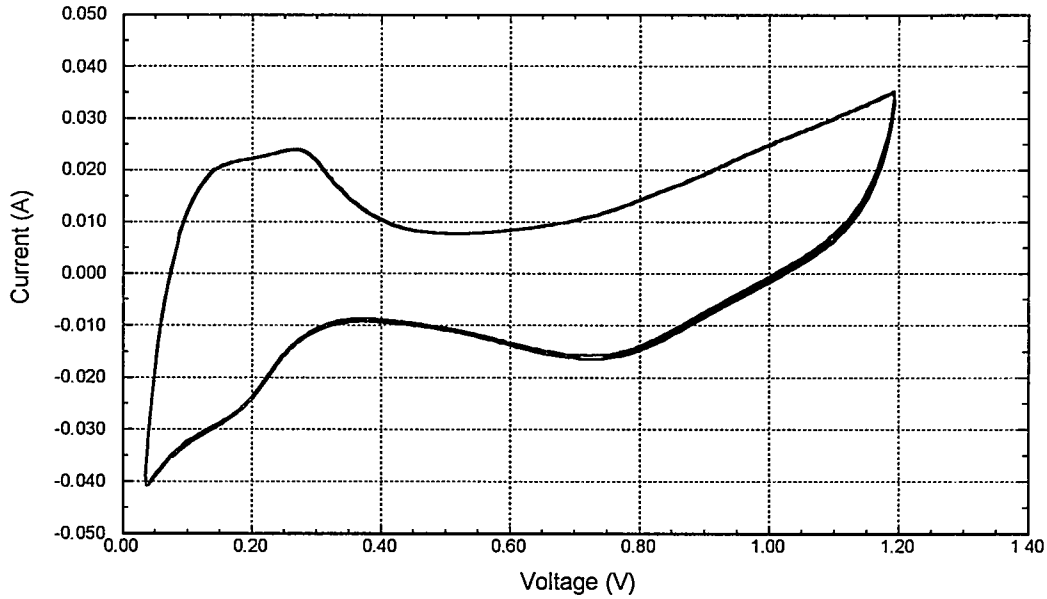

Figure 4-4. Hydrogen adsorption/desorption voltammogram for the anode catalyst of cell 2.

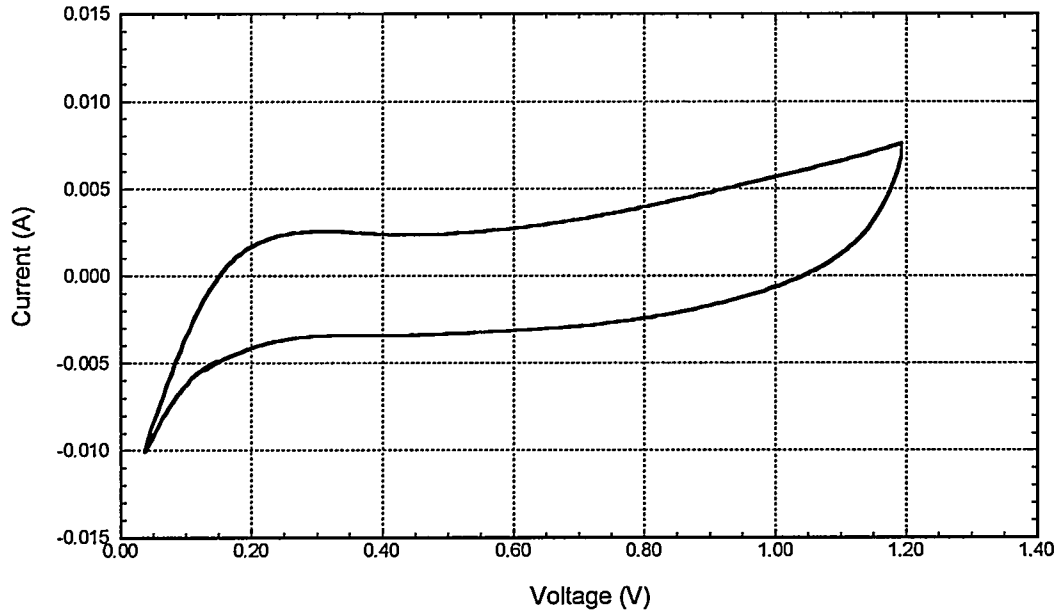

Figure 4-5. Hydrogen adsorption/desorption voltammogram for the cathode catalyst of cell 1.

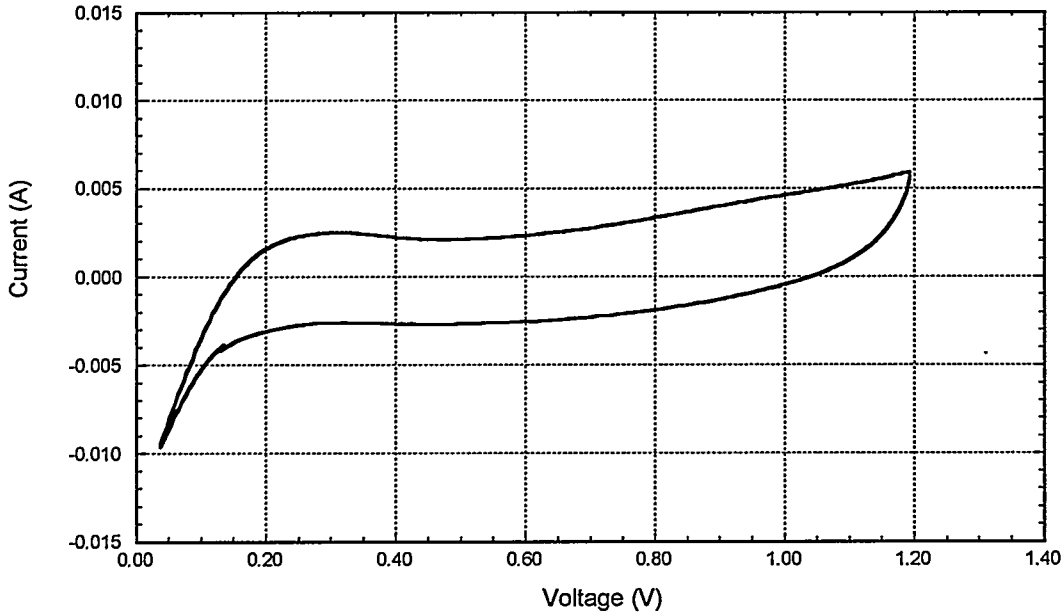

Figure 4-6. Hydrogen adsorption/desorption voltammogram for the cathode catalyst of cell 2.

Table 4-1. Measured Catalytic Surface Areas

Cell #	Electrode	Surface Area (cm^2)
1	Anode	176
1	Cathode	4.5
2	Anode	304
2	Cathode	11.1

4.3 Fuel Cell Measurements

Fuel cell measurements were made using a mixture of hydrogen and air and a mixture of hydrogen and oxygen. A Hewlett Packard load bank was used to measure the power output of the cell. The measurement technique is similar to one described elsewhere.[2]

The cell produced open circuit voltages of about 0.8 to 0.9 V per cell; however, upon load the cell was not able to produce current greater than 0.2 amps (total) regardless of voltage. Thus a fuel cell polarization curve could not be made. No anode to cathode cross-over leak was observed.

4.4 Electrolytic Polarization Measurements

Electrolytic polarization measurements were made at varying temperatures from ambient to 90 °C and are shown in Figure 4-7. The overpotential required for water electrolysis is reduced at the higher temperatures (lower overall cell voltage). The causes are two-fold: increased kinetics at higher temperatures, and increased membrane conductivity at higher temperatures. Using the slope of the polarization curves, the cell resistance can be estimated. This is shown in Figure 4-8 as a function of temperature. A large decrease in cell resistance occurs with the initial temperature increase; then the cell conductivity plateaus at about 70 °C. The decrease in cell voltage above 70 °C is solely due to increased electrode kinetics. The resistances are summarized in Table 4-2.

The electrolytic polarization curves show an unusual discontinuity at about 0.225 A/cm^2 at 40 °C which increases in current density with increasing temperature. This was also observed with the separate MEA used in the micro flow cell (see Figure 3-5).

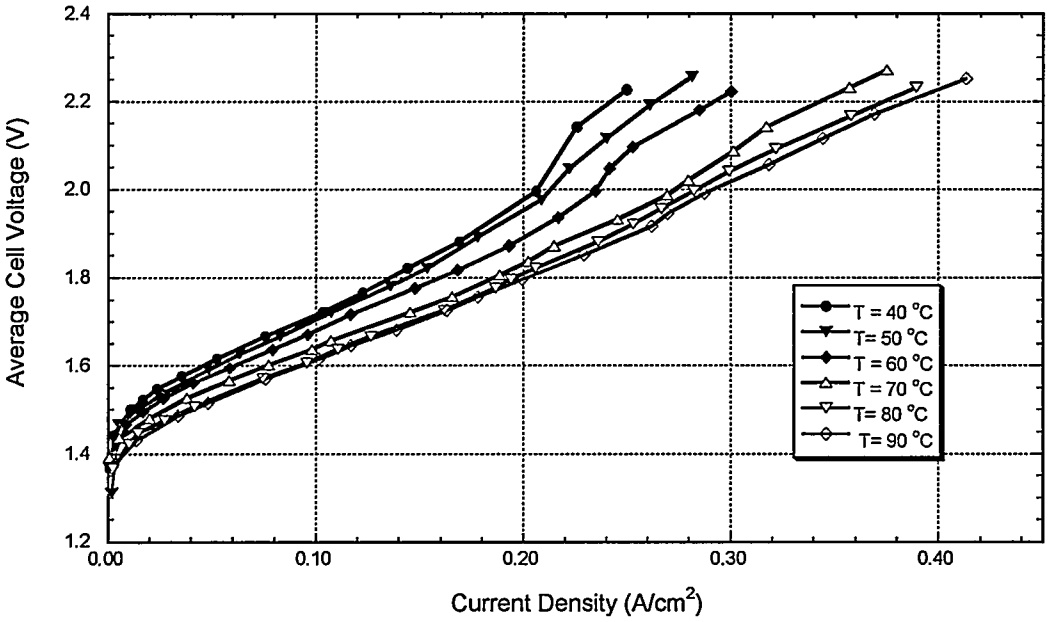

Figure 4-7. Electrolytic polarization curves for the two-cell stack over the temperature range from 40 °C to 90 °C.

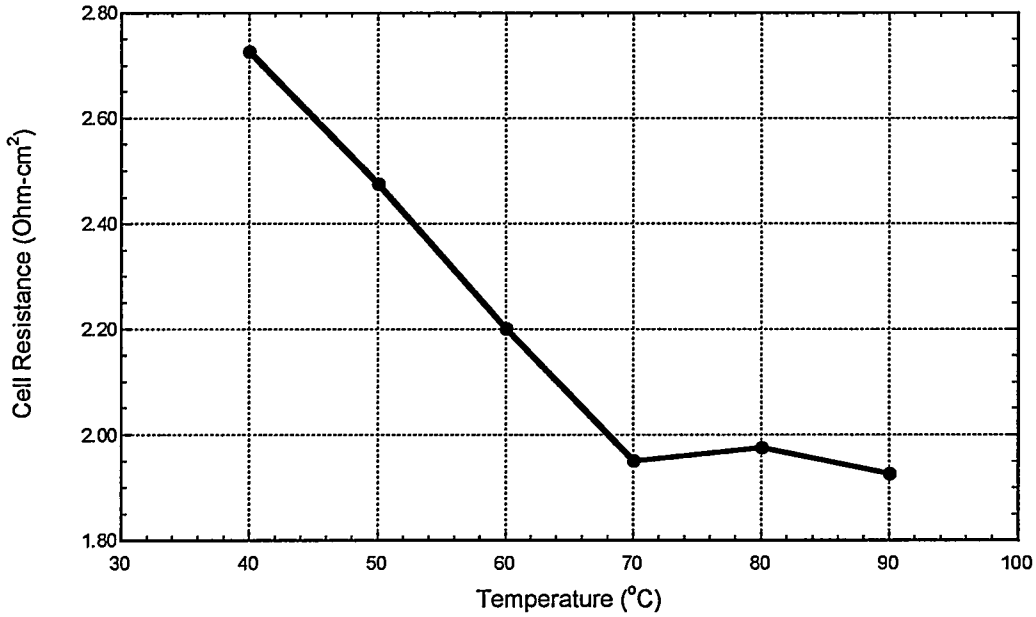

Figure 4-8. Estimated cell resistance determined from the measured polarization curves as a function of temperature.

Table 4-2. Calculated Cell Resistances

T (°C)	R (ohm)	R (ohm-cm^2)
40	0.109	2.725
50	0.099	2.475
60	0.088	2.2
70	0.078	1.95
80	0.079	1.975
90	0.077	1.925

4.5 Discussion

The regenerative fuel cell did not work in the fuel cell mode, while it did perform in electrolytic mode. The performance in the electrolytic mode was similar to the end cells of the 13 cell large electrolyzer and to the separate MEA in the micro flow cell.

The surface area measurements indicated that little electrochemically active platinum was available on the cathode for the fuel cell reaction, and the cell did not perform in fuel cell mode. However the "normal" performance of the cell in electrolytic mode makes this an apparent discrepancy. One major difference in the modes of operation is that when the cell is in the regenerative mode of operation, liquid water is fed to both the anode and the cathode. Liquid water is conductive to protons and probably electrons. When the cell is operated in the fuel cell mode (or during the surface area measurements) only humidified gases are used; thus any proton movement must occur through an ionomer or on a surface. This is one possible explanation of why the cell did perform in electrolytic mode, but not in fuel cell mode, and did not show high platinum surface areas on the cathode.

5.0 Regenerative Fuel Cell Test Facility

5.1 Introduction

The Regenerative Fuel Cell Test Facility provides the framework for evaluating components of a regenerative fuel cell system either as individual components, or collectively as a system. Thus, the facility has the necessary hardware and data acquisition and control to evaluate electrolyzer performance, fuel cell stack performance, or the performance of a regenerative fuel cell combining both functions. Hydrogen storage components can be added to evaluate the performance of an overall regenerative fuel cell system. The modular design of the test system allows for different components to be tested easily in combination. A schematic of the Regenerative Fuel Cell Test Facility is shown in Figure 5-1. The schematic shows the experimental setup for a separate electrolyzer and fuel cell stack with hydrogen storage. The test facility can be configured to test these components separately. The electrolyzer and fuel cell test sections are described in the following paragraphs.

5.2 Electrolyzer Test Section

The portion of the facility dedicated to operating and evaluating electrolyzers includes the electrolyzer, a DC power supply, a temperature-controlled recirculating water system, hydrogen and oxygen separators, and hydrogen and oxygen flow metering and pressure control. The key operating parameters of the electrolyzer test section are identified in Table 5-1.

Table 5-1. Electrolyzer Test Specifications

Testing Parameter	Value
Hydrogen Generation Pressure	1000 psia
Oxygen Generation Pressure	300 psia
Temperature Range	0 °C to 100 °C
Maximum Power Input	9 kW; 30 V at 300 A
Maximum Cooling Load	10 kW Thermal (at stack temperature)
DI Water Quality	> 10^5 ohm-cm water

An electronic DC power supply supplies direct current to the electrolyzer. Current is monitored across a shunt, while the electrolyzer stack voltage is measured across its input terminals. Individual electrolyzer cell voltages are monitored continuously where the design of the electrolyzer permits access to the individual cells. Measurement of the single cell voltages allows identification of defective cells, such as those that may have developed a leak. Single cell voltage monitoring thus serves as a means of monitoring safe operation of an electrolyzer.

Liquid water is supplied to the anode of the electrolyzer by a recirculating deionized water loop incorporating an electric-driven pump and a deionized water resin filter. Typical electrolyzer operation uses the recirculating water loop for waste heat removal. In this test facility, the operating temperature of the electrolyzer is controlled by controlling the temperature of the water loop using a heat exchanger and an electric heater. The electric heater serves to bring the system up to operating temperature and the heat exchanger removes waste heat to maintain the operating temperature.

Hydrogen evolved from the cathode during electrolyzer operation passes through a hydrogen separator to remove entrained liquid water and then through a secondary condenser and water knock-out drum to further ensure complete water removal. The hydrogen exhaust then passes through an EMCO Digital-Valve® which can serve a dual role as a back pressure regulator on the cathode side of the electrolyzer and as a high resolution flow meter. The EMCO Digital-Valve® employed here is a 12-bit binary flow element valve designed for flow control and measurement with a resolution of 0.024% up to a maximum flow of 50 SLPM hydrogen. The maximum back pressure that can be applied is 50 atm (735 psia). The hydrogen exhausted from the EMCO Digital-Valve® then can be stored in a hydrogen storage vessel (not implemented yet) or be exhausted to the hydrogen vent through a back pressure regulator.

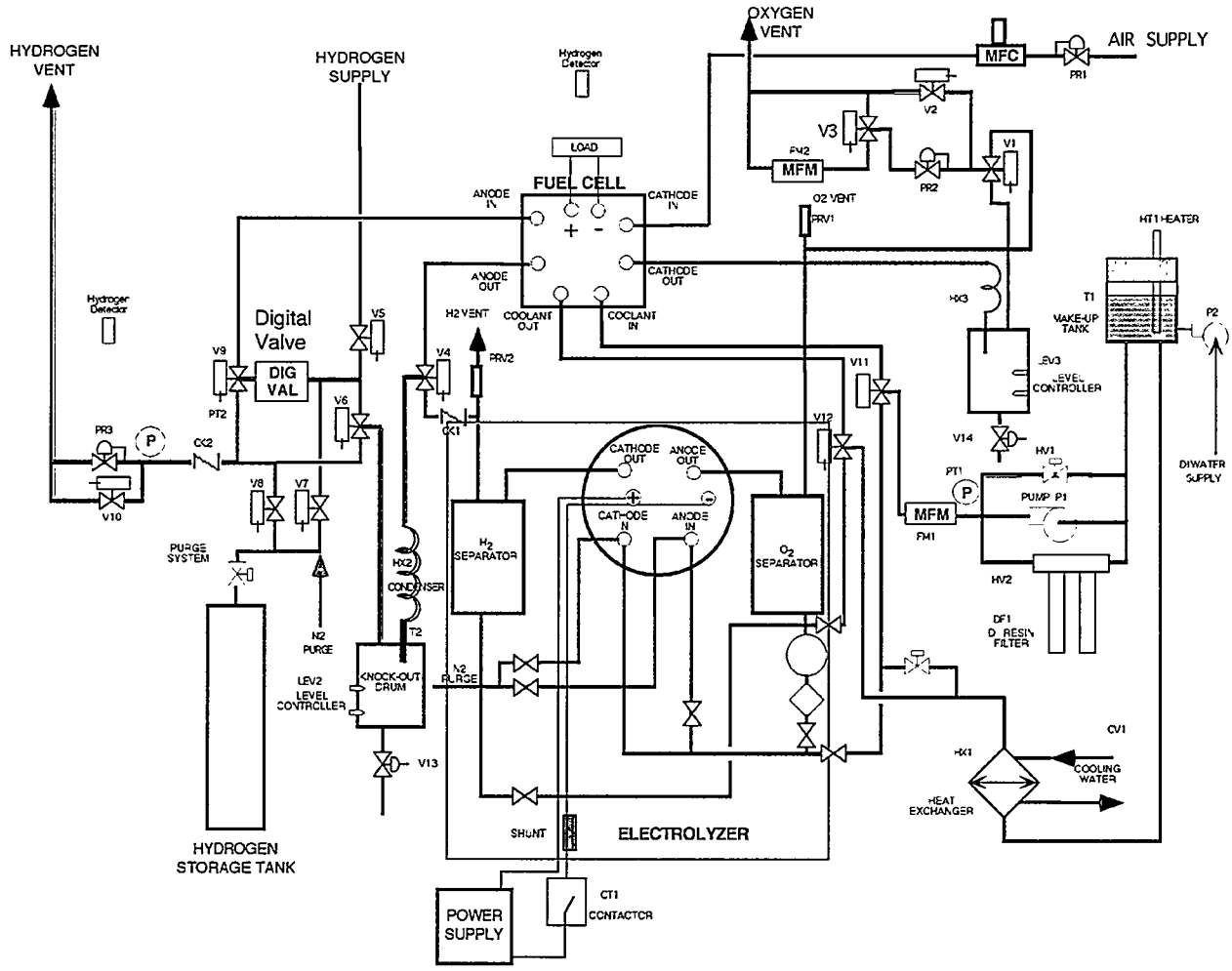

Figure 5-1. Schematic of the Regenerative Fuel Cell Test Facility showing the configuration for testing a separate electrolyzer and fuel cell stack with hydrogen storage.

Oxygen evolved from the cathode during electrolyzer operation is removed from the recirculating water loop through an oxygen separator. The oxygen stream passes through a back pressure regulator that maintains the desired back pressure on the anode. The oxygen then passes through a mass flow meter to the oxygen vent. Oxygen storage currently is not implemented on this system.

5.3 Fuel Cell Stack Test Section

The portion of the facility devoted to evaluation and operation of fuel cell stacks includes the fuel cell stack, a DC electronic load, a deionized water stack cooling loop, hydrogen flow control and supply, and an air flow control and supply. The key operating parameters of the fuel cell stack test section are identified in Table 5-2.

Table 5-2. Fuel Cell Stack Test Specifications

Testing Parameter	Value
Anode Operating (Hydrogen) Pressure	50 psig maximum
Maximum Hydrogen Flow	200 SLPM
Cathode Operating Pressure	50 psig maximum
Maximum Air Flow	1000 SLPM
Temperature Range	0 °C to 100 °C
Maximum Power Output	10 kW; 500 A at 20 V
Maximum Cooling Load	10 kW Thermal (at stack temperature)
DI Water Quality	> 10^5 ohm-cm water

The DC electronic load for the fuel cell stack is a pulse-width modulator with a water-cooled resistor as its electrical energy sink. The load is operated in current control mode with the current measured as a voltage drop across a calibrated shunt. The resulting stack voltage is measured across the terminals of the fuel cell stack. Individual cell voltages are monitored where voltage taps on the individual cells are available. Similar to the electrolyzer, single cell monitoring allows identification of cells that are not functioning properly and thus serves as a means for monitoring safe operation of the fuel cell stack.

Hydrogen can be supplied to the fuel cell stack from either the on-site compressed hydrogen supply or a hydrogen storage tank incorporated as part of a regenerative fuel cell system (when a hydrogen storage system is to be tested). Hydrogen flow is metered to the fuel cell anode through the EMCO Digital-Valve® described in the electrolyzer section. The anode exhaust from the fuel cell stack passes through an exhaust condenser and water knock-out drum and then a back pressure regulator to the hydrogen vent. The back pressure regulator sets the operating pressure of the fuel cell anode.

Air is supplied to the fuel cell stack from a compressed dry air supply. Mass flow controllers meter the air to the fuel cell stack cathode. The cathode exhaust passes through an exhaust condenser, water knock-out drum, and then a back pressure regulator to the oxygen vent line. The back pressure regulator sets the operating pressure of the fuel cell stack cathode.

Fuel cell stack waste heat is removed by a deionized water cooling loop. A pump circulates the water through the fuel cell stack and a heat exchanger with a temperature controller. This temperature controller sets the operating temperature of the fuel cell stack. A Coriolis mass flow meter measures the coolant flow rate. Deionized water quality is maintained by an ion exchange resin filter.

6.0 Russian Electrolyzer

6.1 Description

A 5 kW PEM electrolyzer was supplied by Vladimir Fateev at the RRC Kurchatov Institute in Moscow. The electrolyzer was obtained through Sandia National Laboratories under the RAFCO program.

The operating specifications of the electrolyzer as given by the manufacturer are listed in Table 6-1. The electrolyzer contains 13 cells each with an active area of 500 cm^2. The polymer electrolyte membranes are made of a modified MF-4SK membrane similar to Nafion (see Section 3.0 for an analysis of the components). The bipolar plates are made of titanium and the current collectors are made of porous titanium. The electrolyzer stack end plates are stainless steel. The seals use fluorinated rubber.

Table 6-1. Operating Specifications of the Russian 5 kW Electrolyzer

Parameter	Unit	Value
Hydrogen Production	Nm^3/h	1.10
Oxygen Production	Nm^3/h	0.55
Energy Consumption, max	kW	5.0
Current Density, max	A/cm^2	0.4
Voltage, max (at 85 °C)	V	< 25
Design Temperature	°C	Up to 85-90
Design Pressure	MPa	0.5
Water Electric Resistivity	ohm-cm	$2 \cdot 10^6$
Dimensions of System	cm	100 × 75 × 140
Weight of System	kg	275

The electrolyzer was shipped as a system including the electrolyzer, hydrogen and oxygen separators, a water circulating pump, an ion-exchange filter, and associated tubing and instrumentation. The manufacturer's diagram of the system is shown in Figure 6-1. A picture of the electrolyzer system as installed in the Regenerative Fuel Cell Test Facility is shown in Figures 6-2 and 6-3. The electrolyzer system includes pressure gauges to monitor the pressure in the hydrogen separator for the cathode side of the electrolyzer and the oxygen separator for the anode side of the electrolyzer. Level sensors monitor the water level in the oxygen and hydrogen separators. K-type thermocouples measure anode and cathode outlet temperatures and temperatures at 4 locations within the stack through the anode and cathode inlet and outlet ports. A wire feedthrough connection provides voltage taps to monitor the single cell voltages for the 13 cells in the electrolyzer stack.

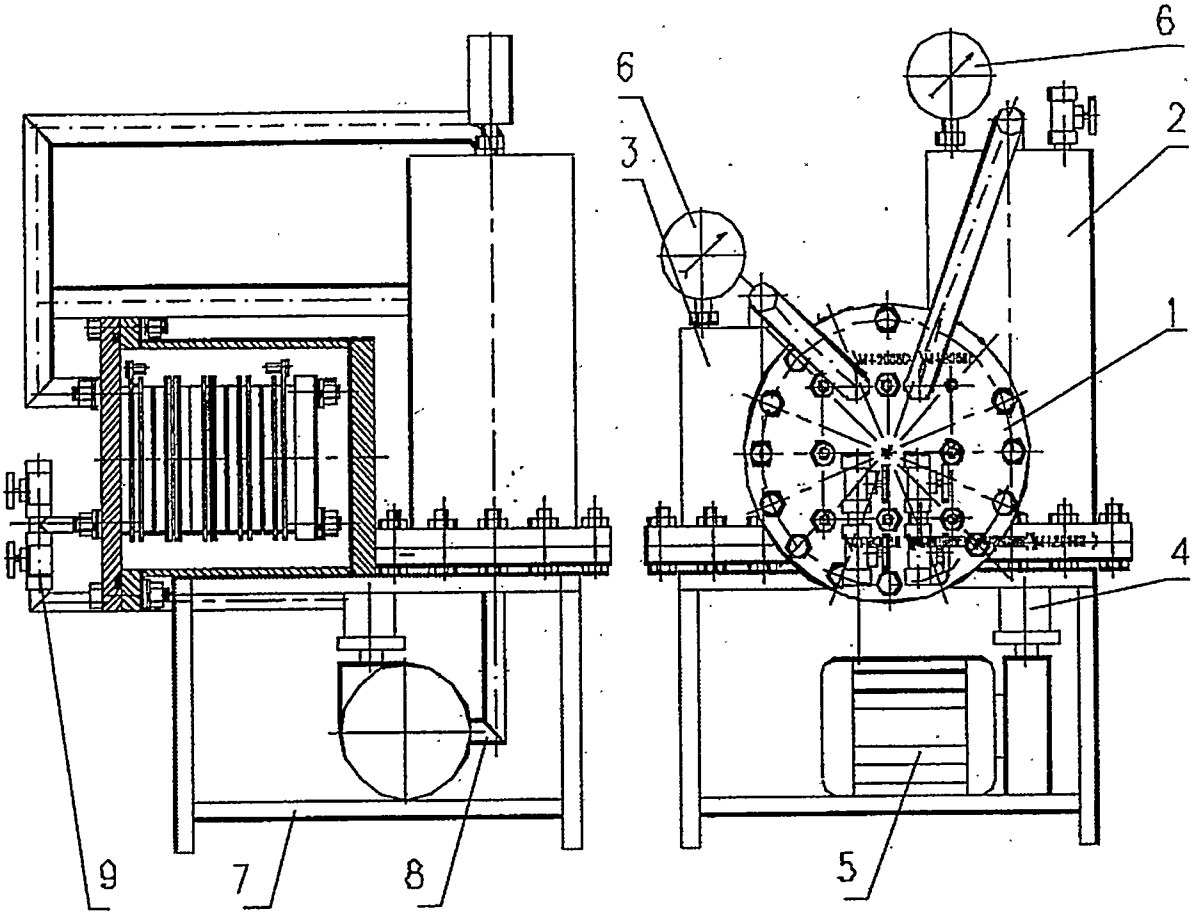

Figure 6-1. Manufacturer's diagram of the electrolyzer system showing a side view with an electrolyzer cross section on the left and a front view on the right. The components are identified as follows: 1) electrolyzer unit, 2) oxygen separator, 3) hydrogen separator, 4) ion-exchange filter, 5) pump, 6) pressure gauges, 7) frame, 8) tubing, and 9) valves. Not shown are the level sensors (in the hydrogen and oxygen separators) and the heater (in the oxygen separator).

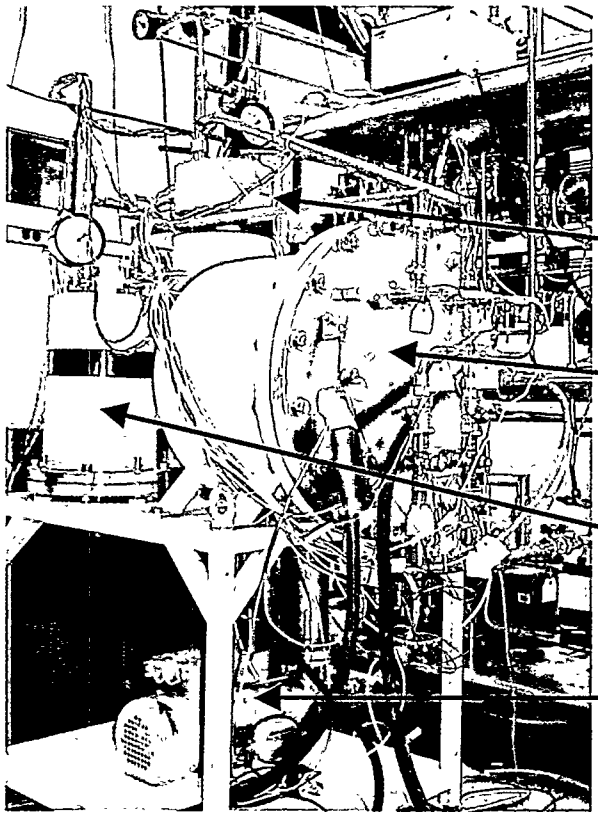

Figure 6-2. Photograph of the Russian 5 kW electrolyzer as installed in the test facility.

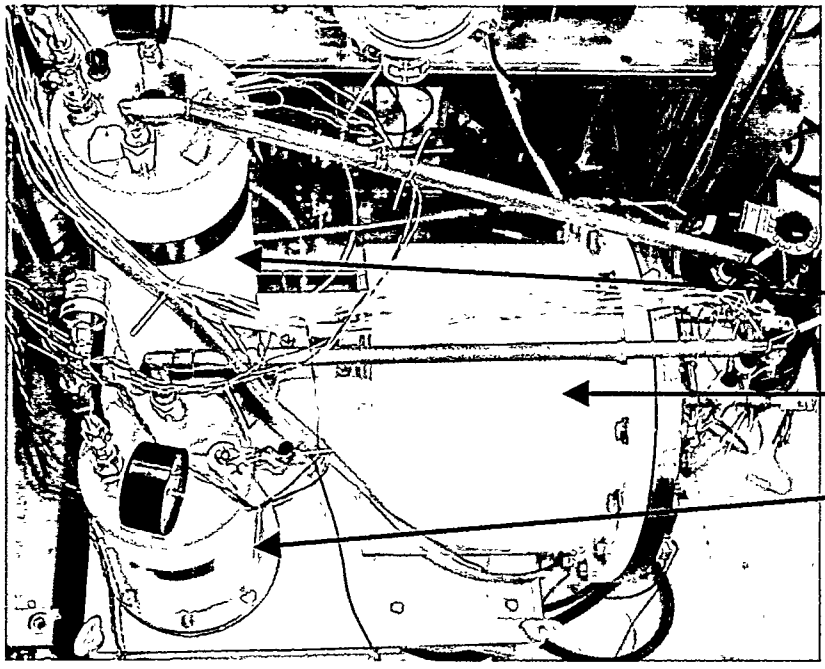

Figure 6-3. Photograph showing an overhead view of the Russian 5 kW electrolyzer as installed in the test facility.

6.2 Manufacturer's Acceptance Test

A set of acceptance tests on the 5 kW PEM electrolyzer were conducted at the RRC Kurchatov Institute in Moscow prior to its shipment. A leakage test was conducted to measure the crossover between the anode and cathode. The measured leak rate for the fully hydrated electrolyzer was reported to be about 1.0 ml/min at 20 °C and 30 psi differential between the anode and cathode chambers. Pressure and leak testing were conducted by pressurizing the vessel and the hydrogen and oxygen separators to 2 MPa for 10 minutes. The manufacturer reported that no leaks or deformation of the vessels were detected.

The operation of the electrolyzer was verified through testing under its normal operating procedure. The electrolyzer system was operated for a total of 50 hours at a hydrogen production rate of 18 SLPM (maximum current input at 200 A) at ambient pressure and a water temperature of 84 °C. The total stack voltage decreased from 23.8 V at the start of testing to 22.7 V at the conclusion of testing. The cell voltage profile at the end of testing is shown in Figure 6-4. The voltages lie between 1.7 and 1.8 V as listed in Table 6-2.

Table 6-2. Cell Voltages at the Conclusion of the Acceptance Test

Cell	1	2	3	4	5	6	7	8	9	10	11	12	13
Voltage	1.74	1.73	1.73	1.74	1.73	1.80	1.70	1.77	1.73	1.73	1.72	1.80	1.77

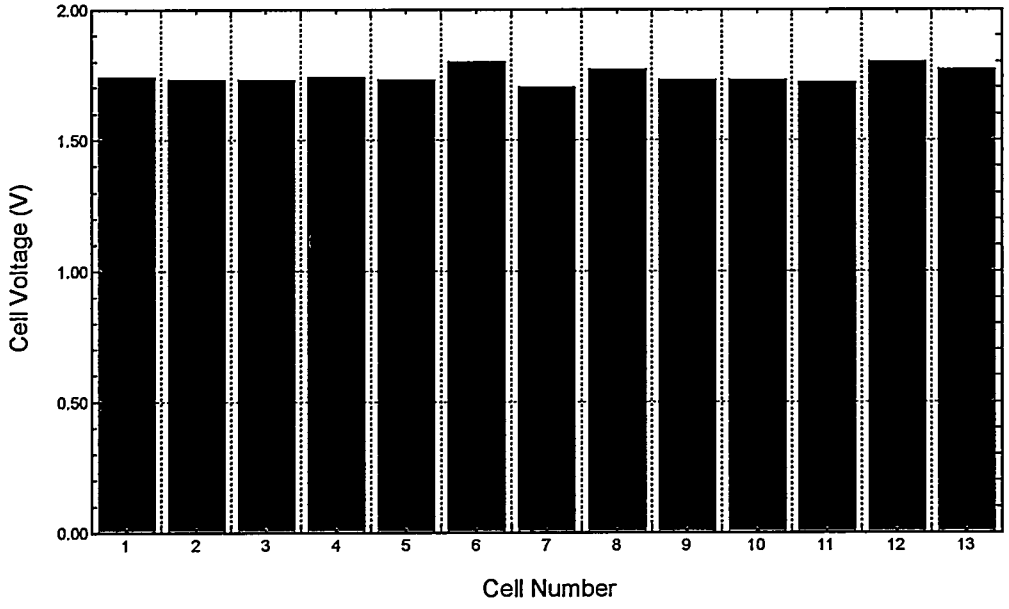

Figure 6-4. Cell voltage profile at the end of acceptance testing as reported by the manufacturer.

7.0 Russian Electrolyzer Experiments

7.1 Experimental Setup

The Russian electrolyzer was installed in the Regenerative Fuel Cell Test Facility following closely the directions provided by the manufacturer. The schematic of the test facility as configured for these experiments is shown in Figure 7-1. The deionized water system of the electrolyzer system was tied into the facility deionized water system. The pump supplied with the electrolyzer system was bypassed because the facility did not have the proper electric supply (380 VAC-3 phase) required by the pump. The deionized water recirculating pump of the test facility was used in its place. The heater in the oxygen separator was supplemented by an additional heater in the water recirculating loop to help raise the water loop to the electrolyzer operating temperature more rapidly. The electrolyzer cathode exhaust was plumbed into the facility hydrogen pressure control, flow measurement, and exhaust system. The electrolyzer anode exhaust was plumbed into the oxygen pressure control and exhaust system. The instrumentation of the electrolyzer, the thermocouples, level sensors, and single-cell voltage monitor was wired into the facility data acquisition and control system. Pressure transducers were added to monitor the anode and cathode pressures. The data acquisition and control software written in National Instruments LabVIEW was modified to provide data acquisition and control of the Russian electrolyzer.

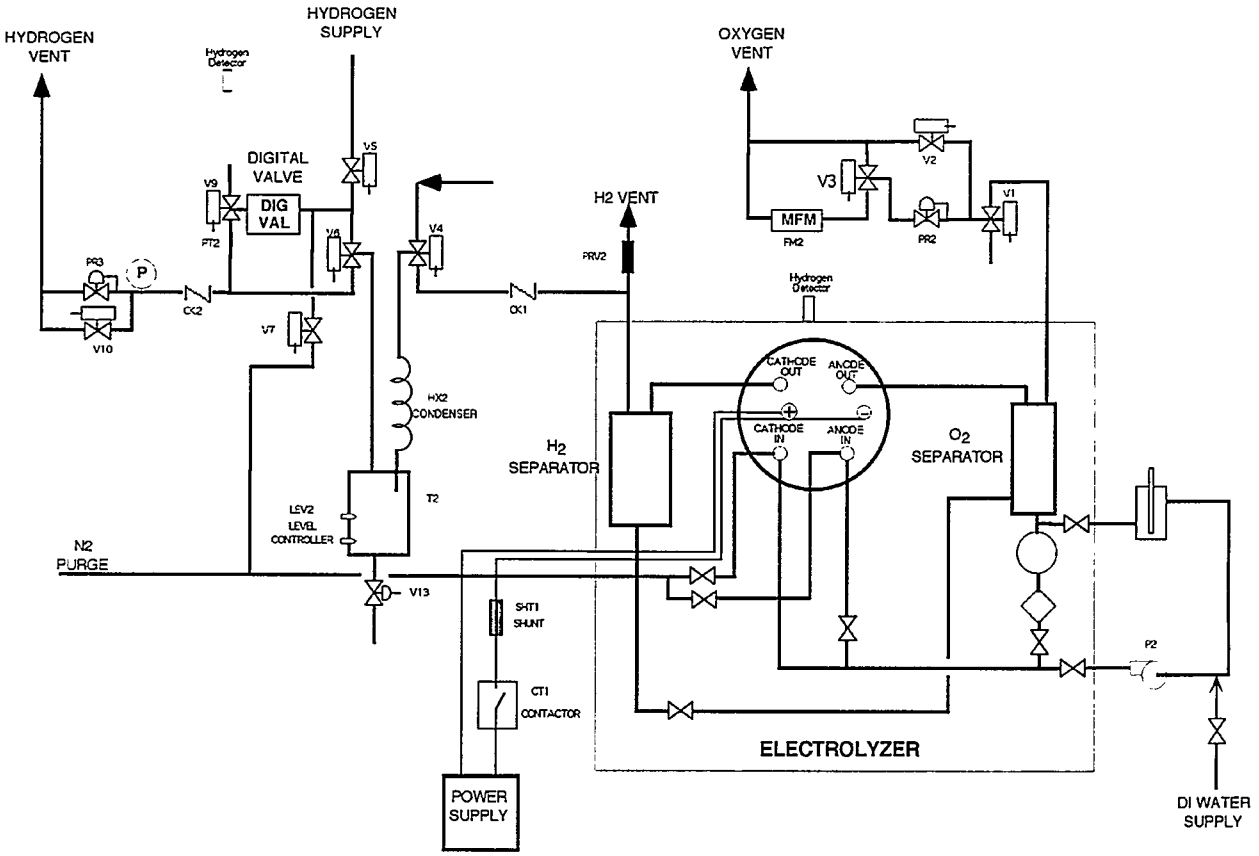

Figure 7-1. Schematic of the experimental setup for the testing of the Russian electrolyzer.

7.2 Experimental Results

The performance of the Russian electrolyzer was mapped over its operating range. The series of experiments conducted thus far have served to verify the operation of the electrolyzer and the functioning of the Regenerative Fuel Cell Test Facility. The experiments were conducted following the start-up, operating, and shutdown procedures provided by the manufacturer. The goal of the initial series of experiments was to characterize the effect of pressure and temperature on the electrolyzer performance.

Figure 7-2 shows the cell voltage of each cell in the electrolyzer at a current density of 0.412 A/cm^2. In general the cell voltage is constant throughout the electrolyzer with the exception of the two stack end cells, cell 1 and cell 13. These two cells, independent of normal operating conditions, show a higher voltage for the electrolysis reaction.

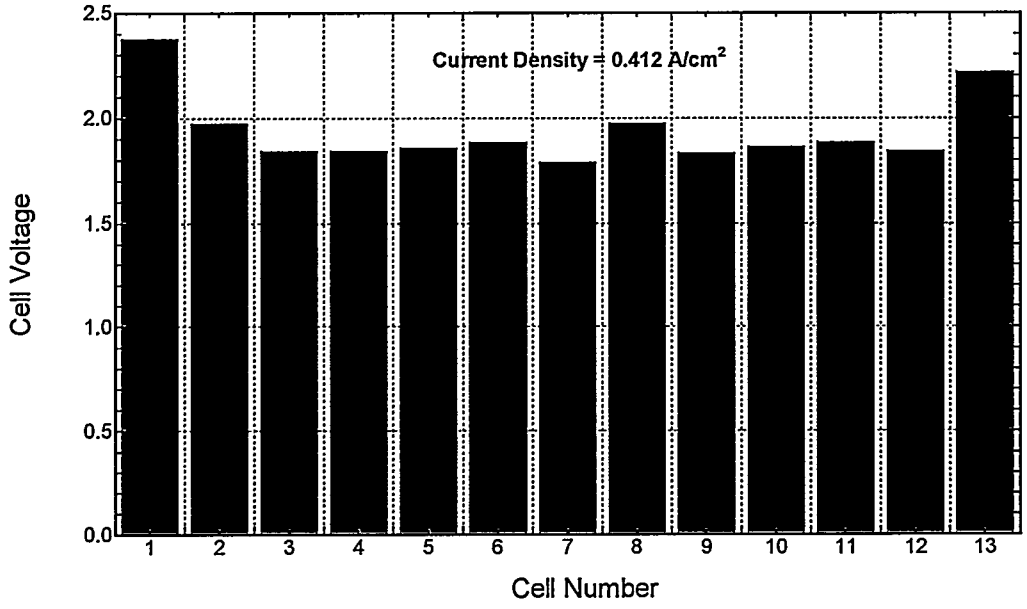

Figure 7-2. Bar chart showing cell voltages for each cell at a current density of 0.412 A/cm^2.

The individual cell polarization curves for T = 85 °C and P = 40 psig are shown in Figure 7-3. The data in Figure 7-3 also shows that the cell voltages are mostly uniform with the exception of the two end cells. From the data shown in Figure 7-3 it is also clear that the polarization slopes of cell 1 and cell 13 are much higher than the slopes of the other cells, indicating that the resistance of these cells is much higher. Calculating the cell resistance from Figure 7-3, we find that cell 1 and cell 13 have more than twice the average cell resistance of the other cells (see Table 7-1). It is possible that the stack is not perfectly uniform in temperature, with the end cells being at a lower temperature which would decrease the membrane conductivity (increasing cell resistance). It is also possible that the stack end plate materials may not be as conductive, and voltage losses could occur in the end plates as the current is collected; however, this is unlikely in view of the manufacturer's acceptance test (see Figure 6-4). Without having further diagnostics it is difficult to decisively determine the cause of the higher end cell overpotentials.

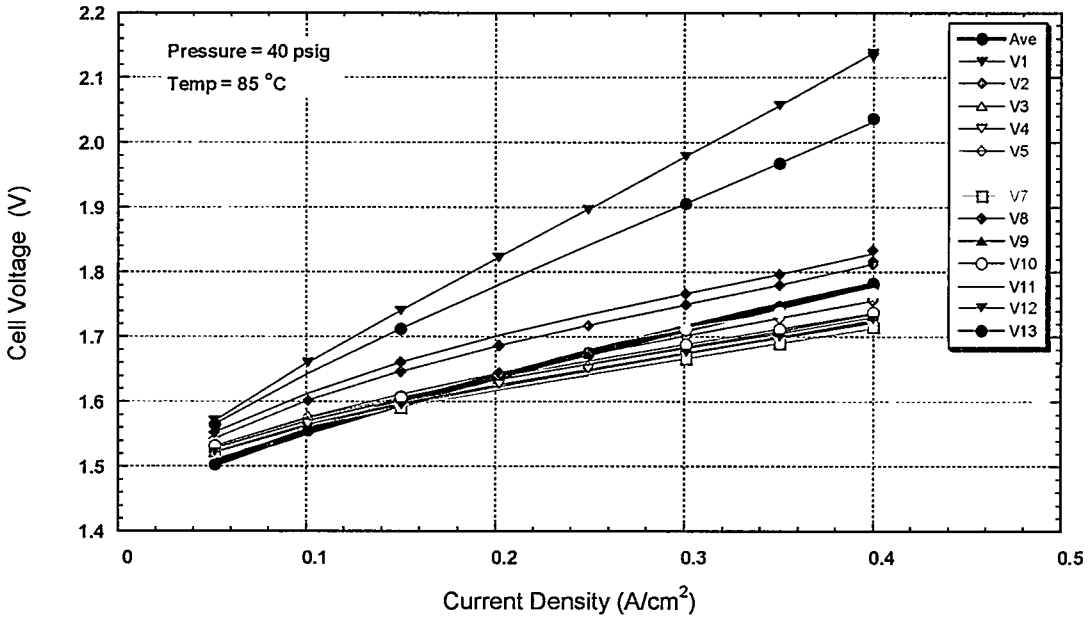

Figure 7-3. Electrolysis polarization curve showing individual cell voltages.

Table 7-1. Calculated Electrolyzer Cell Resistances from the Polarization Curves

Cell	Resistance (ohm)	Resistance (ohm-cm^2)
R1	0.0032	1.6
R2	0.0014	0.7
R3	0.0011	0.55
R4	0.001	0.5
R5	0.0012	0.6
R6	0.0012	0.6
R7	0.001	0.5
R8	0.0015	0.75
R9	0.0011	0.55
R10	0.0011	0.55
R11	0.0011	0.55
R12	0.0011	0.55
R13	0.0026	1.3

Figure 7-4 shows the data from Table 7-1 in a bar chart. It is easy to see that the two end cell have more than twice the average resistance of the average of the other cells. It is also important to note that the average cell resistance of about 0.6 ohm-cm^2 is much higher than that generally measured during high frequency resistance measurements of fuel cell membranes which are generally below 0.2 ohm-cm^2.

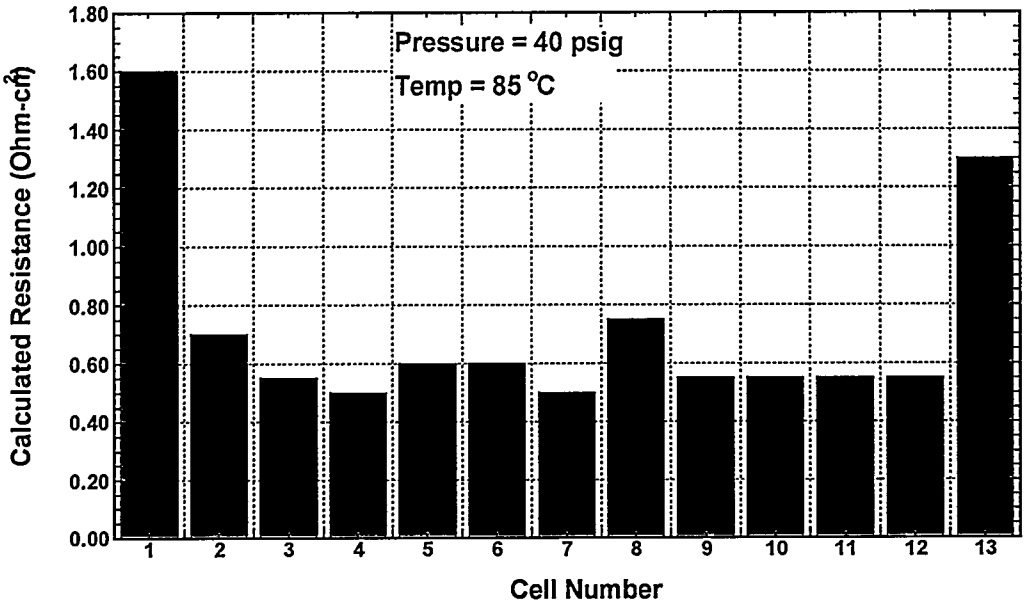

Figure 7-4. Profile of the calculated cell resistances listed in Table 7-2.

The polarization curve for the average cell voltage is shown in Figure 7-5 in a log current format. The cell voltage polarization curves are shown in Figure 7-6 plotted as the individual cell voltages as a function of log current over the range from 1 A to 100 A. We see from this figure that the initial Tafel slope looks linear, which is expected. Looking at the slope of the initial curve (5 A to 10 A) a slope of about 80 mV/decade is measured. This must be considered the Tafel slopes for both the anode and cathode combined. This compares with literature values of 30–40 mV/decade for hydrogen evolution at low current densities and 60 mV/decade for oxygen evolution.[3] So at low current densities one expects an overall Tafel slope of 90–100 mV/decade which compares relatively well with the measured value of 80 mV/decade for this electrolyzer. It should also be noted that the electrode catalysts used in Reference 3 were different electrocatalysts, and thus differences are probably expected. It is also important to note that in Figure 7-6 the initial Tafel slopes for the different cells of the electrolyzer are all essentially identical. This indicates that the electrolyzer cells have identical electrocatalytic formulations, and there are no apparent electrocatalytic kinetic differences between the two end cells and the rest of the electrolyzer stack. This makes it more likely that the differences in cell performance are due to membrane or cell conductivity issues due to electrolyzer stack non-isothermalities.

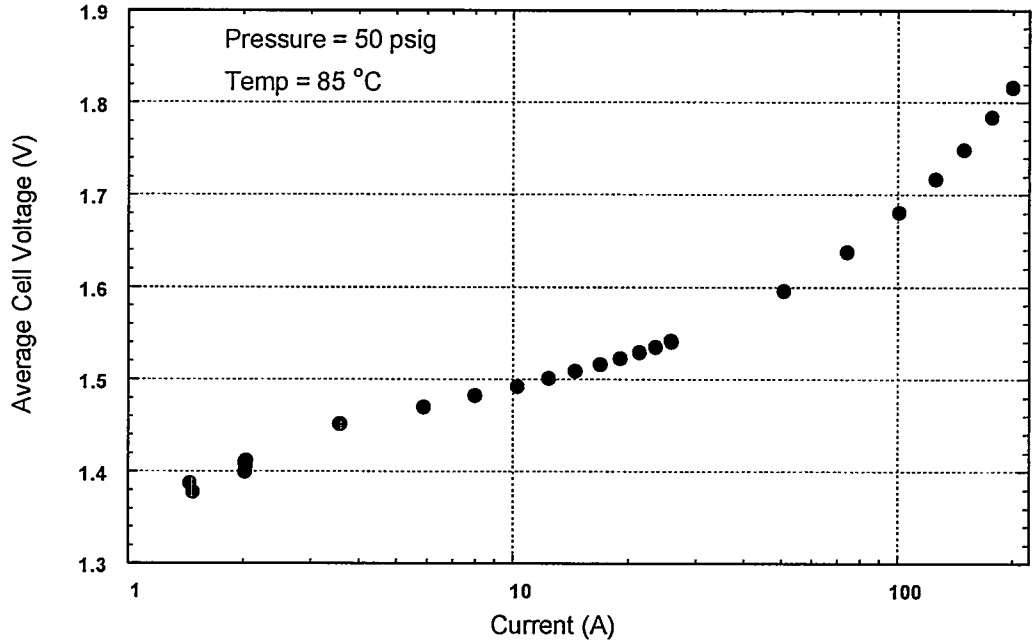

Figure 7-5. Polarization curve showing average cell voltage as a function of ln(Current).

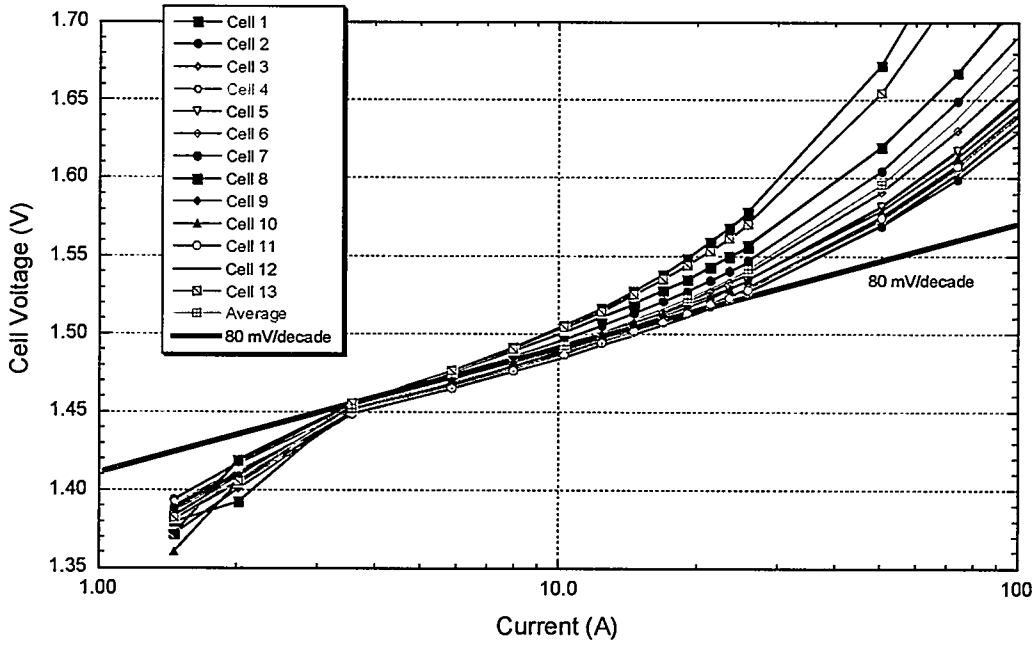

Figure 7-6. Polarization curve showing individual cell voltages as a function of ln(Current).

Figure 7-7 shows the cell voltage for the entire stack as a function of anode temperature. It is obvious that as the temperature increases the electrolyzer performance also increases. This is most likely due to increased membrane conductivity in the electrolyzer. From this figure we can also see that, over the temperature range, cell 1 voltage decreases from 2.40 V to 2.18 V (or 220 mV), cell 13 from 2.21 to 2.04 (or 170 mV) while the average cell voltage decreases from 1.92 to 1.76 (or 160 mV). The best cell, cell 7, decreases from 1.82 to 1.7 (or 120 mV) while the worst of the middle cells, cell 8, decreases from 1.98 to 1.82 (or 160 mV). Thus we see that the more poorly performing the cell is, the larger the increase in performance as the stack temperature is increased. This is a good indication that the stack is not isothermal in its operation.

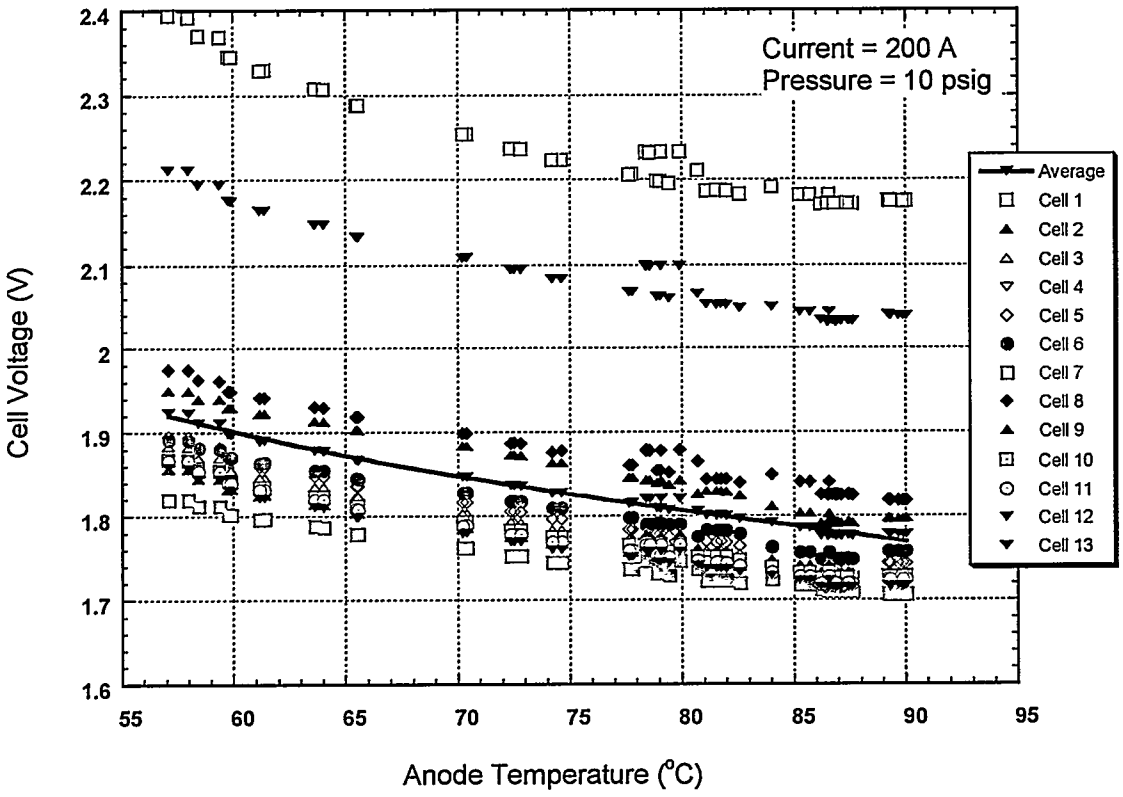

Figure 7-7. Individual cell voltages as a function of anode temperature at a current of 200 A and 10 psig.

Figure 7-8 shows the average cell voltage at five different currents as a function of pressure. Figure 7-9 shows the average cell polarization curve at the different pressures. We see from the polarization curves that there is little pressure dependence. From Figure 7-8, we can see a slight increase in cell voltage as the pressure increases for the different currents; however, the effect is small. The cell voltage is expected to increase as the electrolyzer pressure increases due to additional hydrogen/oxygen partial pressures at the electrocatalysts, and a larger gas permeation of the membrane is also expected.[4] However, over this relatively small pressure variation, the electrolyzer performance is essentially uniform.

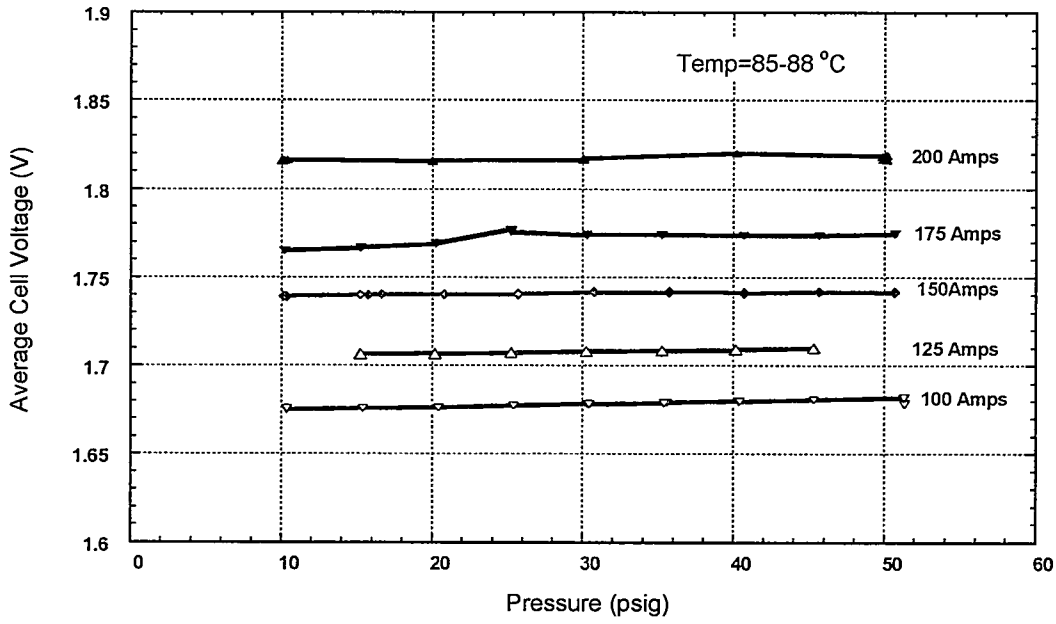

Figure 7-8. Average cell voltage as a function of pressure at 5 currents.

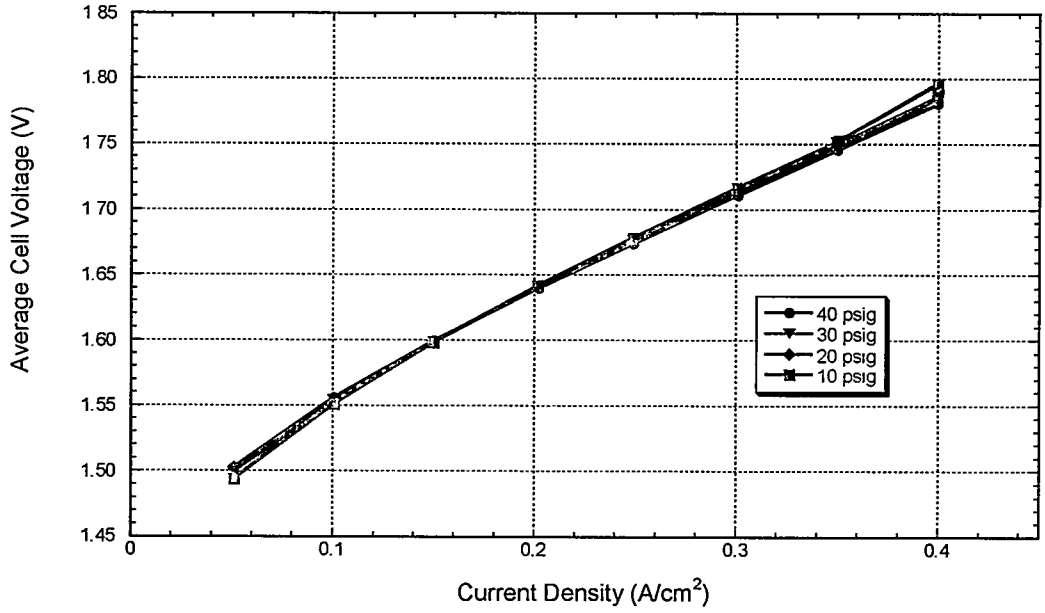

Figure 7-9. Polarization curves showing the average cell voltage as a function of current density at four pressures.

Figure 7-10 shows the measured and calculated hydrogen flow rate out of the electrolyzer for various power inputs into the electrolyzer. The agreement between the measured and calculated values is good indicating that the test performance and calibrations are good, and that little hydrogen is lost via permeation through the membrane. Figure 7-11 shows the hydrogen production efficiency as a function of current density. This shows that the electrolyzer has good production efficiency at low current densities, while as the current density increases the overpotentials increase, the voltage loss due to cell resistance becomes larger, and the production efficiency decreases.

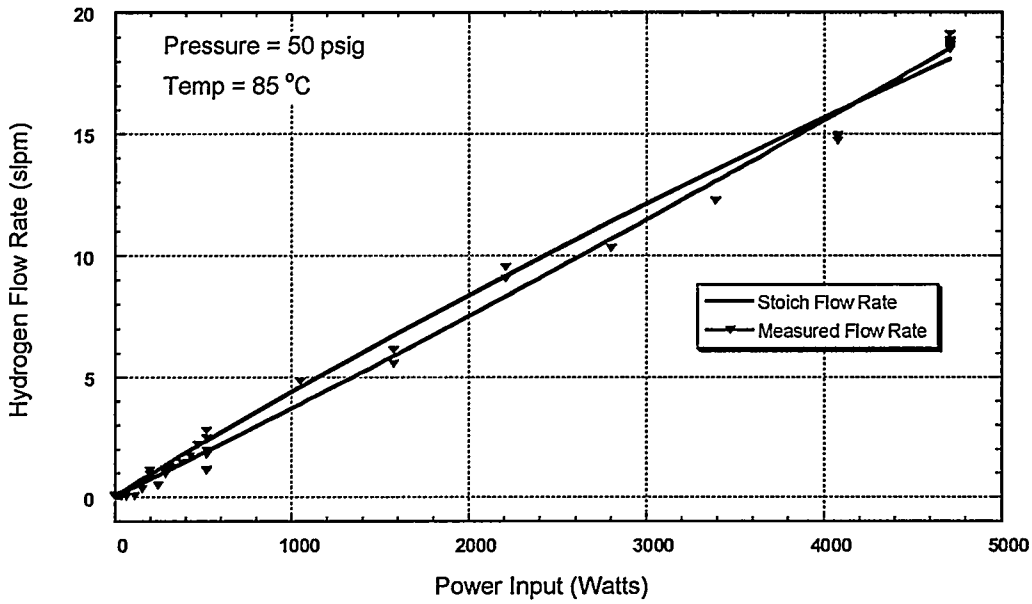

Figure 7-10. Comparison of the stoichiometric and measured hydrogen flow rate as a function of electrolyzer power input.

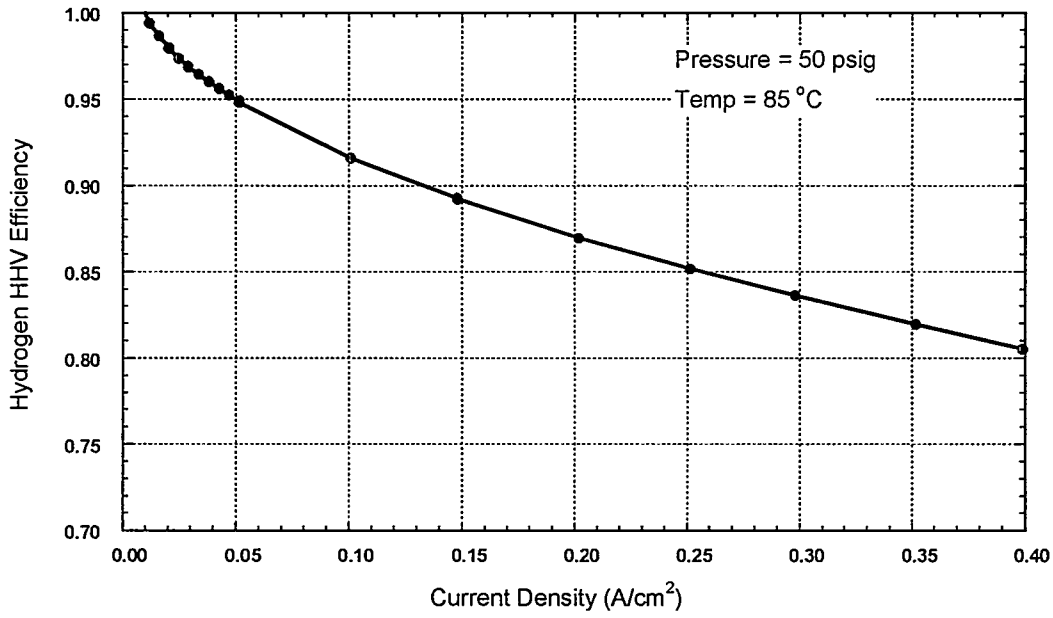

Figure 7-11. Hydrogen HHV efficiency as a function of current density.

8.0 Future Directions

Our future directions include, first, continuing testing of the 5 kW electrolyzer to identify further the operating parameters of the system and to apply advanced diagnostics to identify and understand the mechanisms that limit its performance. We intend to map the operating parameters of the electrolyzer including measurement of the electrolysis polarization curves as a function of temperature and pressure; measurement of the effect of the water feed including rate, temperature, and impurities; and also measurement of detailed energy and mass balances on the system. Testing can also be done on simulated energy inputs from wind and solar energy generation. These provide data that can be used for modeling of an electrolyzer-fuel cell regenerative system. We also will employ advanced diagnostics including AC impedance techniques to measure membrane resistance, low current testing to examine the electrode kinetics, and adding diluents to measure anode and cathode overpotentials. These diagnostics would give us a fundamental understanding of the electrolyzer performance and identify limitations and possible improvements in performance. It is also important to measure the effects of adding "depolarizing" agents to reduce the electrode overpotential such as methane on the cathode.

Secondly, we will continue to conduct research in regenerative fuel cells. In the near term, this will involve a rebuild of the 2-cell regenerative fuel cell stack and mapping of its operation and testing using the advanced diagnostic techniques such as AC impedance. Data obtained will be used in a regenerative fuel cell system model to compare system performance with a system with separate fuel cell and electrolyzer. In the longer term, we will develop a full-scale regenerative fuel cell stack containing 10–20 cells. This task will include design, building, and testing of the regenerative fuel cell stack and computer simulation of the stack performance in a system.

Thirdly, we will build upon our regenerative fuel cell test stand to develop an in-house capability to test regenerative fuel cell systems and their components. In the near term, we can use in-house or commercially available components such as the Russian electrolyzer, a fuel cell stack, and a hydrogen storage device to test the system test stand framework. Testing provides validation of the test stand and also provides data for development of a regenerative fuel cell system model. In the long term, the RFC system test stand provides the framework for development and testing of system components such as electrolyzers, fuel cells, hydrogen storage and compression, and regenerative fuel cells. In conjunction with the system model, the test stand can be used for investigating options for system architecture and operation.

These proposed activities will allow us to investigate the feasibility of regenerative fuel cell systems, provide a basis for comparison with other alternative energy storage options, and provide the scientific and engineering basis for commercial regenerative fuel cell systems.

References

1. Borup, R. L. and Vanderborgh, N. E., Proceedings of the Electrochemical Society (1995), No. 95-23 (Proton Conducting Membrane Fuel Cells I), 167-81.
2. Weisbrod, K. R. and Vanderborgh, N. E., Proceedings of the 29th Intersociety Energy Conversion Engineering Conference (1994), 855.
3. Andolfatto et al., *Int. J. Hydrogen Energy*, 19 (1994) 421.
4. Ledjeff et al., *Int. J. Hydrogen Energy*, 19 (1994) 453.